Journal of Computational Physics 228 (2009) 1275–1293

Contents lists available at ScienceDirect

Journal of Computational Physics

journal homepage: www.elsevier.com/locate/jcp

Micromixing models for turbulent flows

Daniel W. Meyer [a,*], Patrick Jenny [b]

[a] Department of Energy Resources Engineering, Stanford University, Green Earth Sciences Building, Room 65, 367 Panama Street, Stanford, CA 94305, USA
[b] Institute of Fluid Dynamics, ETH Zurich, Switzerland

ARTICLE INFO

Article history:
Received 2 June 2008
Received in revised form 13 October 2008
Accepted 14 October 2008
Available online 25 October 2008

MSC:
65C35
65C20

PACS:
02.70.Uu
47.27.Eq
47.70.Fw
82.20.Wt
82.33.Vx

Keywords:
Mixing model
Micromixing model
Molecular mixing
PDF method
FDF method
PSP
IEM
Curl
Mapping closure
EMST

ABSTRACT

In transported probability density function and filtered density function methods, micromixing models are required to close the molecular mixing term. The accuracy and computational efficiency of improved versions of the parameterized scalar profile (PSP) model are assessed and compared with commonly used mixing models such as Curl, modified Curl, interaction by exchange with the mean and Euclidean minimum spanning tree. Different generalizations of the PSP mixing model for spatially inhomogeneous flow configurations are presented. The selected test cases focus on molecular mixing and avoid interference with other models. Simulation results for a three-stream problem, involving two inert scalars, and a multi-scalar test case with mean-scalar-gradients are presented.

1. Introduction

1.1. Modeling turbulent transport and mixing

Turbulent transport and mixing are important in many flows and relevant in disciplines such as biology, geosciences or chemical engineering. Reviews about mixing of scalars (such as temperature and chemical compositions) in turbulent flows are given in [1,2] and in chapter 3 of [3]. During a turbulent mixing process, scalar interfaces are continuously stretched and

* Corresponding author. Tel.: +1 650 721 2644; fax: +1 650 725 2099.
E-mail address: meyerda@stanford.edu (D.W. Meyer).

0021-9991/$ - see front matter © 2008 Elsevier Inc. All rights reserved.
doi:10.1016/j.jcp.2008.10.019

folded, and complex small-scale scalar structures involving high concentration gradients are formed. Depending on the Schmidt number, the smallest lengthscales are typically of the same order or smaller as those of the flow field. At these small scales, molecular diffusion becomes dominant and scalar fluctuations are reduced locally. In high Reynolds number flows at sufficiently large Schmidt number (e.g. $Re_\lambda = 500$ and $Sc = 1$), where the energy containing scalar lengthscales are much larger than the diffusive ones, this process is governed by the generation of small-scale scalar gradients through turbulence and becomes independent of the molecular diffusivity [3,4]. In turbulent flow fields, despite similarities between velocity and scalar statistics there exist important differences, e.g. local anisotropy [1,2,5] and effects due to differential diffusion [6,7]. Since these phenomena occur at the smallest scales, the resulting wide range of scalar field lengthscales is difficult to resolve in numerical simulations. Mainly three different approaches are used for the simulation of turbulent mixing in engineering applications.

In Reynolds averaged Navier–Stokes (RANS) simulations, transport equations of statistically averaged quantities like the mean flow velocity $\langle \mathbf{U} \rangle$ and the mean scalar vector $\langle \boldsymbol{\phi} \rangle$ are solved. In reactive flows, the closure of the average chemical source term

$$\langle S_\alpha(\boldsymbol{\phi}) \rangle = \int S_\alpha(\boldsymbol{\psi}) f(\boldsymbol{\psi}; \mathbf{x}, t) d\boldsymbol{\psi} \tag{1}$$

is most difficult. Here, the scalar vector is defined as $\boldsymbol{\phi} \equiv (\phi_1, \ldots, \phi_\alpha, \ldots, \phi_{n_s})^T$, where n_s is the number of scalars and S_α is the source term due to chemical reaction in the conservation equation of the scalar ϕ_α. Note that the exact determination of $\langle S_\alpha(\boldsymbol{\phi}) \rangle$ requires the knowledge of the joint composition probability density function (PDF) f at every point $\boldsymbol{\psi}$ in sample space. The sample space or in the present context more precisely the scalar space is spanned by all physically possible values of the scalar vector $\boldsymbol{\phi}$. In composition PDF methods, a transport equation for $f(\boldsymbol{\psi}; \mathbf{x}, t)$ is formulated (Eq. (6.27) in [3]) and typically solved with a Lagrangian particle method. Correspondingly $\langle S_\alpha(\boldsymbol{\phi}) \rangle$ can be evaluated according to Eq. (1) without closure assumptions. However, mixing due to turbulent convection and molecular diffusion require modeling. The latter appears in the PDF transport equation as the conditional average $\langle \Gamma_{(\alpha)} \nabla^2 \phi_\alpha | \boldsymbol{\psi} \rangle = \langle \Gamma_{(\alpha)} \nabla^2 \phi'_\alpha | \boldsymbol{\psi} \rangle + \Gamma_{(\alpha)} \nabla^2 \langle \phi_\alpha \rangle$ with the diffusion coefficient Γ_α. Note that the Einstein summation convention does not apply to indices in brackets. The first term on the right hand side is often referred to as micromixing and accordingly corresponding closure models are called mixing models. Note that $\phi'_\alpha \equiv \phi_\alpha - \langle \phi_\alpha \rangle$ is the scalar fluctuation and $\langle \cdot \rangle$ is an averaging operator.

In joint velocity–composition PDF methods not only the chemical source term but also convective turbulent transport appear in closed form (Section 3.5 in [8]). Various models for the effects of the fluctuating viscous stresses and the fluctuating pressure gradients were proposed, including the generalized and the refined Langevin models, both reviewed by Pope in Section 5 of [9]. In addition to the high level of closure, joint velocity–composition PDF methods provide much more statistical information compared to moment closure models. However, like in joint composition PDF methods, a model is required for the closure of the molecular mixing term, which involves $\langle \Gamma_{(\alpha)} \nabla^2 \phi'_\alpha | \mathbf{V}, \boldsymbol{\psi} \rangle$. In compressible low Mach number flows, a transport equation for a density weighted PDF, called mass density function (MDF), is solved (Eq. (3.59) in [8]).

Due to the continuous increase in computer power, large eddy simulations (LES) of reactive flows become more and more popular. Instead of taking the ensemble average of the Navier–Stokes equations (to obtain the RANS equations) spatial filtering is applied, which leads to similar closure problems [3,10]. Here, the modeling task consists in capturing the effects of the unresolved dynamics of the subgrid scales. With respect to the closure of the filtered chemical source term, the following two approaches are used among others. In the linear eddy model (LEM) by Kerstein [11], the unresolved subgrid scales are modeled by solving a one-dimensional reaction–diffusion problem in each LES grid cell. The problems in the different grid cells are coupled by advective transport. Since all chemical and diffusion lengthscales are resolved in the one-dimensional problems, this approach is computationally expensive (Section 4.3 of [3]). Alternatively, Colucci et al. [12] outlined an approach based on a filtered density function (FDF). The FDF contains information about the scalar distribution in the filter volume at any point in the computational domain. An FDF transport equation was derived, where the chemical source term appears in closed form (Eq. (25) in [12]). Since the FDF and the PDF have similar properties and since their transport equations have a similar structure, the FDF equation can be solved with a similar stochastic particle method. Likewise, the same mixing models seem to be applicable [13,14].

Therefore and in agreement with a very recent comment by Raman and Pitsch [14, p. 1719], mixing models developed for transported PDF methods are of certain relevance for LES in connection with FDFs. Even though considerable efforts have been made to improve mixing models, there is still room for improvement: recently, Pope [15] wrote: 'Mixing models should remain an active area of research for some time, since they are a crucial element in PDF methods in both RANS and LES approaches, and current models have several well-appreciated shortcomings.' A very similar quote can be found at the beginning of chapter 6.6.5 in the book by Fox [3]. The modeling difficulties arise from the complicated nature of molecular diffusion (p. 58 in [9]), which leads to a set of requirements an ideal mixing model should fulfill (e.g. boundedness, localness, linearity and independence). A list of these requirements is given in Chapter 6.6 of [3] or in [16].

1.2. Different mixing models

One of the earliest mixing models for particle PDF methods is the coalescence and dispersion (CD) model by Curl [17], dating back to 1963. Originally Curl developed this model to describe mixing of colliding droplets with different concentrations in a two-liquid suspension. Consequently Curl's model can easily be integrated into a stochastic particle framework as

used for PDF simulations. In each time step, particle pairs are randomly selected and their individual concentrations set to their average value. Other early approaches are summarized by Dopazo [18] and Janicka et al. [19]. Later, a modified CD (MCD) model, where two particles mix gradually and not completely like in the CD model, was devised [19]. There, the mixing intensity is random for each particle pair. In both models, the mixing rate is adjusted through the number of pairs that mix per time step. The main disadvantage of these models is that the PDF of an inert scalar does not become Gaussian in homogeneous turbulence. Furthermore, the particle trajectories in scalar space are not continuous over time and therefore, these models are not even in a weak sense local (Norris and Pope [20, p. 212]). A more detailed discussion about localness follows later in this section.

The most widely used mixing model is based on a contribution by Villermaux and Devillon [21] and is called interaction by exchange with the mean (IEM) mixing model (also known as the linear mean-square estimation (LMSE) model [22]). This model is based on the simple fact that molecular mixing reduces scalar fluctuations and draws instantaneous scalar values towards their local mean. While the IEM model correctly predicts that the variance of an inert scalar decays in homogeneous turbulence, it is not able to describe the evolution of the scalar PDF appropriately, i.e. the shape of the PDF is preserved and it does not approach a Gaussian distribution.

Based on the work of Ottino [23] about mixing of lamellar structures, Fox [24–26] developed Fokker–Planck (FP) equation based mixing models. Here, if multiple scalars are to be considered, boundedness is a non-trivial issue, as was noted by Pope [8] at the end of Section 5.2.4 for a simpler FP model. Boundedness reflects the physical limits with respect to the spreading of mixture states in scalar space. For example in a spatially homogeneous mixing scenario, which involves multiple inert scalars that have equal diffusion coefficients, the region in scalar space occupied by all mixture states does not grow over time.

A different branch of model development was initiated by the mapping closure (MC) model of Pope [27]: starting from a Gaussian reference field, where the scalar gradient statistics conditioned on the scalars are known, molecular diffusion in a so-called surrogate field is obtained through a mapping. The core assumption here is that the statistics of the scalar and the surrogate field are identical. Even though the MC formulation was successfully validated against the one-scalar direct numerical simulation (DNS) of Eswaran and Pope [28], the proposed extension for multi-scalar mixing scenarios is problematic. It is based on an ordering of scalars, which introduces unphysical scalar dependences as mentioned after Eq. (93) in [27]. The MC model is local in a strong sense, meaning that only neighboring particles in scalar space interact with each other. This property is advantageous especially for reactive scalars with strongly localized reaction zones [29,20]. Later an algorithmic extension of Pope's MC particle implementation for multiple scalars was devised by Subramaniam and Pope [16]. The localness of the MC model was generalized by replacing the one-dimensional ordering in scalar space by an Euclidean minimum spanning tree (EMST). The EMST model is local for the particles participating in the mixing process during a given time step. These particles are a subset of the available particles, which is determined by an intermittency process that was introduced to avoid so-called stranding. Stranding refers to an unphysical accumulation of particles on lines forming a tree-like structure in scalar space. A different generalization of the single scalar MC to multiple scalars was proposed by Klimenko and Pope [30]: their extension is based on a unification of conditional moment closure (CMC) and PDF methods and is called multiple mapping conditioning (MMC). MMC is of special value for applications, where the majority of the accessible scalar states lie on a manifold with reduced dimensionality. This is the case in most combustion applications. The reported results for the so-called three-stream problem are in good qualitative agreement with the DNS data by Juneja and Pope [7], where mixing of two inert scalars in homogeneous turbulence is considered. However, there remain some open issues: linearity and independence are not fully satisfied and so far, the method was only applied to homogeneous problems [31]. Mixing model issues are addressed in [32]. It has to be pointed out that MMC is not only a mixing model but rather an entire framework for scalar transport problems.

Recently, Meyer and Jenny [33] proposed a mixing model, which is based on a parameterization of one-dimensional scalar profiles (PSPs). The approach of modeling molecular mixing by considering scalar profiles at the diffusive scales is very natural and in fact not new. The contribution of Fox [24] based on Ottino [23] was already mentioned and the work of Peters and coworkers [34,35] points in a similar direction. Furthermore, there is a certain relation between the LEM [11] and the PSP model: like in the LEM, we model the unresolved scalar field lengthscales by a scalar distribution along one spatial coordinate. The solutions for the diffusion problems of the PSPs, however, are simple algebraic expressions, whereas in the LEM, detailed diffusion problems are solved at higher computational cost. The PSP model is not linear with respect to multiple scalars and the particle implementation described in [33] is only applicable for spatially homogeneous cases.

The models discussed so far can be classified into different categories: Subramaniam and Pope [16] introduced the particle-interaction mixing-model category. Except the FP-based models all mixing models mentioned so far belong to this category. A different categorization was introduced by Pope [9]: he distinguishes between deterministic and stochastic models. Here, the IEM and MC models are deterministic, whereas models like CD, MCD, FP, EMST, and PSP are stochastic mixing models. Note that the EMST model is a stochastic mixing model because of the random intermittency feature.

For the mixing models outlined here, a mixing timescale τ_ϕ has to be provided. In this respect not much has changed since the review by Pope [8] in 1985: Spalding's suggestion of using $\tau_\phi = \tau/C_\phi$ is employed in most cases, where C_ϕ is a model constant, representing the mechanical-to-scalar timescale ratio, and τ is the integral turbulence timescale. This choice leads to a model for the scalar dissipation which reads $\varepsilon_\phi = \frac{1}{2}C_\phi\langle\phi'^2\rangle/\tau$ (Eqs. (5.23) in [8] and (4.93) in [3]). Unfortunately C_ϕ is not a universal constant. It is mainly influenced by the state of the scalar energy spectrum and the presence of chemical

reactions. Illustrative examples showing the influence of the scalar energy spectrum are shown in Figs. 13 and 14 of [28] and [7], respectively: starting with a scalar field containing essentially one scalar lengthscale, the scalar spectrum in the DNS equilibrates after about six eddy turnover times and the mechanical-to-scalar timescale ratio reaches a stationary value $C_\phi \approx 2.5$ independent of the initial lengthscale. In Chapter 4.6 of [3], Fox presents a model for the mechanical-to-scalar timescale ratio, which can handle non-equilibrium spectrum dynamics at high Reynolds numbers. The second factor can be attributed to a steepening of scalar gradients due to chemical reactions (Section 5.7.5 in [8]). Consequently, a different value for C_ϕ has to be employed, as for the recently published joint PDF calculations of piloted jet flames by Cao et al. [36]. Consistently, the DNS data of a plane jet flame by Hawkes et al. [37] shows significant variation of the scalar dissipation rates of reactive and non-reactive scalars (Section 3.2.4).

Pope [8, p. 172] and Fox [38] proposed variants of Curl's CD and the IEM models, respectively, which are conditional on the velocity. Pope [4] shows that the independence of molecular diffusivity at high Reynolds numbers, mentioned at the beginning of this paper, is closely connected to the velocity conditioning of the molecular diffusion term: mixing models, which include in the joint velocity–composition PDF context no velocity conditioning, are in general unable to satisfy the condition $\langle \Gamma_{(\alpha)} \nabla^2 \phi_\alpha | \mathbf{V} \rangle = 0$. In the high Reynolds number limit, this condition is supported by DNS data of Overholt and Pope [5], where mixing of a passive scalar in homogeneous stationary turbulence with a mean scalar gradient was studied. In practice, however, conditioning on velocity is often ignored in joint velocity–composition PDF calculations [36,39].

In this paper, the accuracy and efficiency of the most widely used mixing models such as CD, MCD, IEM and EMST is assessed and compared with a generalized version of the PSP model. In Section 2, the model formulations are outlined including different generalizations of the PSP mixing model suitable for spatially inhomogeneous mixing scenarios. Moreover, the particle implementation of the MC model is extended for unequally weighted particles and for a single-scalar test case compared with the EMST model. Since turbulent convection is closed in velocity–composition PDF methods, the selected test cases presented in Section 3 focus on molecular mixing. In the two-scalar case presented in Section 3.1, it is shown that it is misleading to infer from the excellent results of the one-scalar MC that the EMST model is able to predict a multi-scalar PDF evolution with similar accuracy. To investigate the scaling of the computational cost with respect to the number of scalars and particles, the multi-variate mean scalar gradient case introduced by Subramaniam and Pope [16] is simulated using different mixing models. Further results are presented in Section 3.2 and conclusions are given in Section 4.

2. Mixing model formulations

In PDF methods, transport equations of multi-variate probability density functions are solved. For example, the transport equation of the joint velocity–composition PDF $f(\mathbf{V}, \boldsymbol{\psi}; \mathbf{x}, t)$, as derived in Chapter 6.2 of [3], reads

$$\frac{\partial f}{\partial t} + V_i \frac{\partial f}{\partial x_i} = -\frac{\partial}{\partial V_i}\left(f \left\langle \frac{\mathrm{D}U_i}{\mathrm{D}t} \middle| \mathbf{V}, \boldsymbol{\psi} \right\rangle \right) - \frac{\partial}{\partial \psi_\alpha}\left(f \left\langle \frac{\mathrm{D}\phi_\alpha}{\mathrm{D}t} \middle| \mathbf{V}, \boldsymbol{\psi} \right\rangle \right). \tag{2}$$

For simplicity gas mixtures with constant density are considered here. Based on the Navier–Stokes and the scalar conservation equations, the substantial derivatives on the right-hand side of Eq. (2) can be replaced, which leads to

$$\frac{\partial f}{\partial t} + V_i \frac{\partial f}{\partial x_i} = \frac{1}{\rho}\frac{\partial \langle p \rangle}{\partial x_i}\frac{\partial f}{\partial V_i} - \frac{\partial}{\partial V_i}\left(f \left\langle \nu \nabla^2 U_i - \frac{1}{\rho}\frac{\partial p'}{\partial x_i} \middle| \mathbf{V}, \boldsymbol{\psi} \right\rangle \right) - \frac{\partial}{\partial \psi_\alpha}\left(f \langle \Gamma_{(\alpha)} \nabla^2 \phi'_\alpha | \mathbf{V}, \boldsymbol{\psi} \rangle \right) - \Gamma_{(\alpha)} \nabla^2 \langle \phi_\alpha \rangle \frac{\partial f}{\partial \psi_\alpha} - \frac{\partial}{\partial \psi_\alpha}[f\, S_\alpha(\boldsymbol{\psi})], \tag{3}$$

where p is the pressure, ρ the density and ν the viscosity. The third and fourth term on the right-hand side of Eq. (3) describe molecular mixing, where the third term has to be modeled with a mixing model. Note that integration of Eq. (3) over the velocity sample space $\mathbf{V}$ leads to a transport equation for the composition PDF $f(\boldsymbol{\psi}; \mathbf{x}, t)$. Due to their high dimensionality, PDF transport equations are generally solved with realization based Lagrangian particle methods [40,10,3]. Each particle i has a set of properties, e.g. a particle position $\mathbf{x}^{(i)}$, a weight $w^{(i)}$ and a scalar vector $\boldsymbol{\phi}^{(i)}$. The evolution of these properties is described by stochastic or deterministic differential equations. Examples of such evolutions are depicted in Fig. 1 for the case of an inert scalar mixing in forced homogeneous turbulence. The PDF at a certain location $\mathbf{x}$ is then approximately represented by a finite number of particles near that position. Therefore, the physical space is discretized into computational grid cells and within each of them statistical homogeneity is assumed. More details about the connection between particle evolution and PDF transport equations are given in Chapter 12.6 of [10] and in Section 4.6 of [8]. From the particle field statistical moments can be extracted, e.g. the mean of the scalar vector $\boldsymbol{\phi}$ in the computational grid cell $\mathscr{V}$ might be estimated as

$$\langle \boldsymbol{\phi} \rangle = \frac{\sum_{\mathbf{x}^{(i)} \in \mathscr{V}} w^{(i)} \boldsymbol{\phi}^{(i)}}{W}, \quad \text{where } W \equiv \sum_{\mathbf{x}^{(i)} \in \mathscr{V}} w^{(i)}. \tag{4}$$

More about estimating statistical quantities can be found in Chapter 12.6.3 of [10], Chapters 7.3.4 and 7.4.4 of [3], and Section 6.7 of [8]. In the following sections, scalar evolution equations of the notional particles are given for different mixing models. These equations are valid for unequally weighted particles and deal with inert scalars. Variable particle weights are required for efficient PDF methods, since it is preferable to keep the number of particles more or less constant per grid cell. This leads to uniformly distributed statistical errors in the computational domain (Chapter 7.3.1 in [3]). Furthermore, they are used in MDF methods for variable-density flows (Section 3.4 of [8]). Note that the following mixing models are

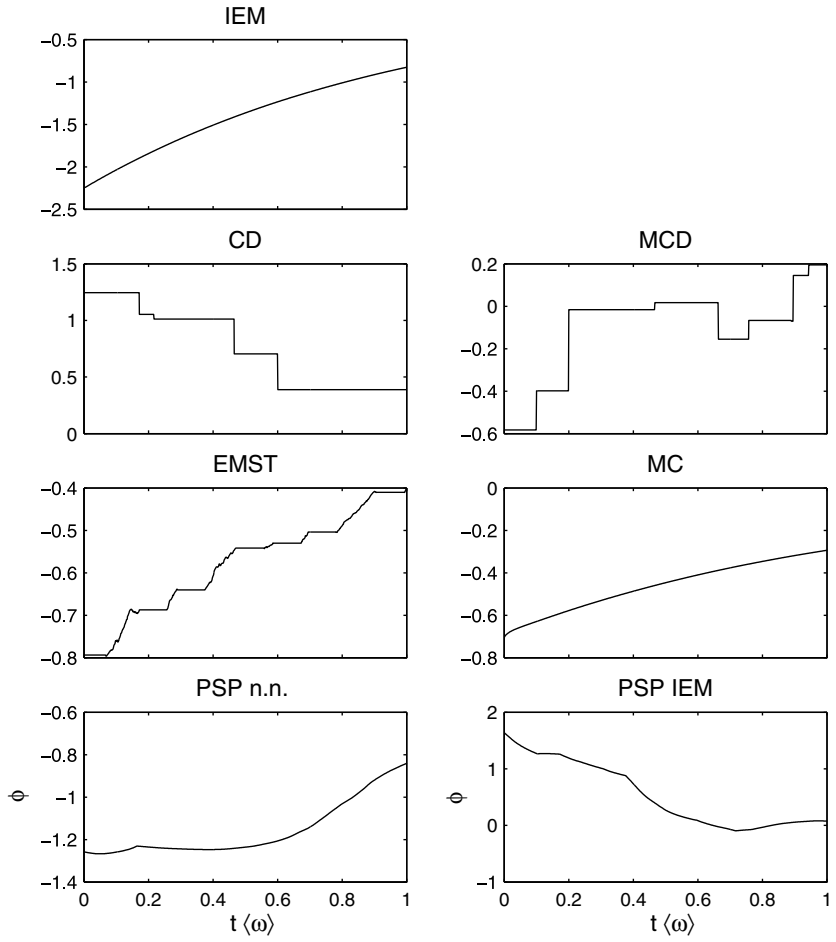

Fig. 1. Scalar trajectories in non-dimensional time $t\langle\omega\rangle$ of a particle using different mixing models; the initial scalar PDF is a Gaussian.

all mass conservative and independent of translations in scalar space. Consequently, $\langle\boldsymbol{\phi}\rangle$ is not affected and it is unimportant whether $\boldsymbol{\phi}$ or $\boldsymbol{\phi}'$ is used for the model formulations.

2.1. Interaction by exchange with the mean (IEM)

Interaction by exchange with the mean [21,22] is the simplest mixing model. In stationary homogeneous turbulence, the scalar values of the particles relax at a constant rate towards the local scalar mean as

$$\frac{d\boldsymbol{\phi}^{(i)}}{dt} = -\frac{1}{2}C_\phi\langle\omega\rangle(\boldsymbol{\phi}^{(i)} - \langle\boldsymbol{\phi}\rangle), \tag{5}$$

where $\langle\omega\rangle$ is the mean turbulence frequency and the constant C_ϕ a simple model for the mechanical-to-scalar timescale ratio as discussed in Section 1.2. In the high-Reynolds-number limit, typically $C_\phi = 2$ is used [3,10]. From Eq. (5) it becomes clear that the IEM model preserves the shape of the scalar PDF since all particles in the ensemble relax towards the mean at the same rate. Consequently, as is shown in Pope [10] (Eq. (12.349)), the IEM mixing model is exact for a Gaussian shaped scalar PDF and a homogeneous turbulent flow field. The decay rate of the scalar variance $\langle\phi_\alpha'^2\rangle$ in stationary homogeneous turbulence can be derived directly from Eq. (5)

$$\frac{d}{dt}\ln\langle\phi_\alpha'^2\rangle = -C_\phi\langle\omega\rangle. \tag{6}$$

In a time marching algorithm, one way to integrate expression (5) is given by the scheme

$$\boldsymbol{\phi}^{(i)q+1} = \left[\exp\left(-\frac{1}{2}C_\phi\langle\omega\rangle\Delta t\right) - 1\right](\boldsymbol{\phi}^{(i)q} - \langle\boldsymbol{\phi}\rangle^q) + \boldsymbol{\phi}^{(i)q}, \tag{7}$$

where Δt is the time-step size and q the time level. Note that this scheme remains stable for large time steps.

2.2. Curl and modified Curl mixing models (CD, MCD)

In Curl's coalescence and dispersion (CD) mixing model [17], during the time step from t^q to t^{q+1} the scalar values of two mixing particles i and j become

$$\boldsymbol{\phi}^{(i)q+1} = \boldsymbol{\phi}^{(j)q+1} = \boldsymbol{\phi}_c \quad \text{with } \boldsymbol{\phi}_c \equiv \frac{w^{(i)}\boldsymbol{\phi}^{(i)q} + w^{(j)}\boldsymbol{\phi}^{(j)q}}{w^{(i)} + w^{(j)}}. \tag{8}$$

This is Eq. (26) in [16], which is a mass conservative generalization of Curl's formulation that was given for equally weighted particles. The mixing rate in a grid cell is controlled by the fraction of participating particle pairs, which is given by the total weight $w_m \approx 2C'_\phi W \Delta t \langle\omega\rangle$ of all particles treated by Eq. (8). Note that C'_ϕ is another model constant. In the modified coalescence and dispersion (MCD) model [19], the particle pairs do not mix completely, i.e. scheme (8) is replaced by

$$\boldsymbol{\phi}^{(i)q+1} = \boldsymbol{\phi}^{(i)q} + h(\boldsymbol{\phi}_c - \boldsymbol{\phi}^{(i)q}) \text{ and } \boldsymbol{\phi}^{(j)q+1} = \boldsymbol{\phi}^{(j)q} + h(\boldsymbol{\phi}_c - \boldsymbol{\phi}^{(j)q}), \tag{9}$$

where $h \in [0,1]$ is a uniformly distributed random variable different for each particle pair. For high Reynolds number flows and equally weighted particles, $C'_\phi = 2$ and $C'_\phi = 3$ for the CD and MCD models, respectively, lead to scalar variance decay rates that are consistent with the one predicted by the IEM model (see Appendix).

2.3. Mapping closure (MC)

Generalizing the particle implementation of the single-scalar mapping closure by Pope [27] for unequally weighted particles is straightforward. The scalar evolution of the particles is given by Eq. (52) in [27],

$$\begin{aligned}
\frac{d\phi^{(1)}}{dt} &= \frac{1}{2}C'_\phi\langle\omega\rangle\left[B_{1+\frac{1}{2}}(\phi^{(2)} - \phi^{(1)})\right] \\
\frac{d\phi^{(i)}}{dt} &= \frac{1}{2}C'_\phi\langle\omega\rangle\left[B_{i+\frac{1}{2}}(\phi^{(i+1)} - \phi^{(i)}) - B_{i-\frac{1}{2}}(\phi^{(i)} - \phi^{(i-1)})\right] \text{for } i = 2,\ldots,n_p - 1 \\
\frac{d\phi^{(n_p)}}{dt} &= \frac{1}{2}C'_\phi\langle\omega\rangle\left[-B_{n_p-\frac{1}{2}}(\phi^{(n_p)} - \phi^{(n_p-1)})\right],
\end{aligned} \tag{10}$$

where the particles are ordered according to their scalar values, $\phi^{(i)} \leqslant \phi^{(i+1)}$, implying localness in scalar space; n_p is the number of particles. The contraction coefficients

$$B_{i+\frac{1}{2}} \equiv \frac{n_p g\left(\eta_{i+\frac{1}{2}}\right)}{\eta_{i+1} - \eta_i} \tag{11}$$

depend on the standard Gaussian PDF g(η), where η is the sample space coordinate with

$$\eta_i \equiv \mathrm{G}^{(-1)}\left(p_{i-\frac{1}{2}}\right) \quad \text{and} \quad \eta_{i+\frac{1}{2}} \equiv \mathrm{G}^{(-1)}(p_i). \tag{12}$$

Here, $\mathrm{G}^{(-1)}$ is the inverse cumulative density function corresponding to the PDF g. The arguments $p_{i-\frac{1}{2}}$ and p_i are given as

$$p_{i-\frac{1}{2}} \equiv \frac{\sum_{j=1}^{i} w^{(j)} - 0.5w^{(i)}}{W} \quad \text{and} \quad p_i \equiv \frac{\sum_{j=1}^{i} w^{(j)}}{W} \tag{13}$$

and depend on the particle weights $w^{(i)}$. Note that equation (13) is a generalization of Eq. (42) in [27] for unequal weights. Based on equation (29) in [27] one can show that for a Gaussian scalar PDF the mapping reduces to a time dependent linear function $X(\eta,\tilde{t}) \sim \eta\exp(-\tilde{t})$, with non-dimensional time $\tilde{t} \equiv \frac{1}{2}C'_\phi\langle\omega\rangle t$. Consequently, the scalar variance decay is the same as in the high Reynolds number limit if $C'_\phi = 2$. With a non-Gaussian scalar PDF, the same value for C'_ϕ results in a different decay rate, however. For stable time integration of the system (10) an implicit Euler scheme is employed. To validate the outlined particle implementation, the solutions of 10 simulations with 10,000 particles each were averaged and compared with the analytical MC solution presented in Section 2.5 of [27] (Fig. 2). Note that the initial PDF is a double-delta-function, in which case the MC mixing model is in very good agreement with DNS data [28]. In all simulations uniformly distributed particle weights ranging from 0.5 to 1.5 and a time-step size of $\Delta t = 0.001/\langle\omega\rangle$ were employed.

2.4. Euclidean minimum spanning tree (EMST) model

The EMST mixing model [16] is an algorithmic extension of the single-scalar MC. Hereby the focus was set on preserving localness: the ordering of the notional particles along the scalar coordinate was replaced by a multi-dimensional EMST. The definition of the contraction coefficients (Eq. (11)) was replaced by a formulation, which is linear with respect to the cumulative particle weights. These are computed along the EMST branches starting from the endings (p. 503 in [16]). This

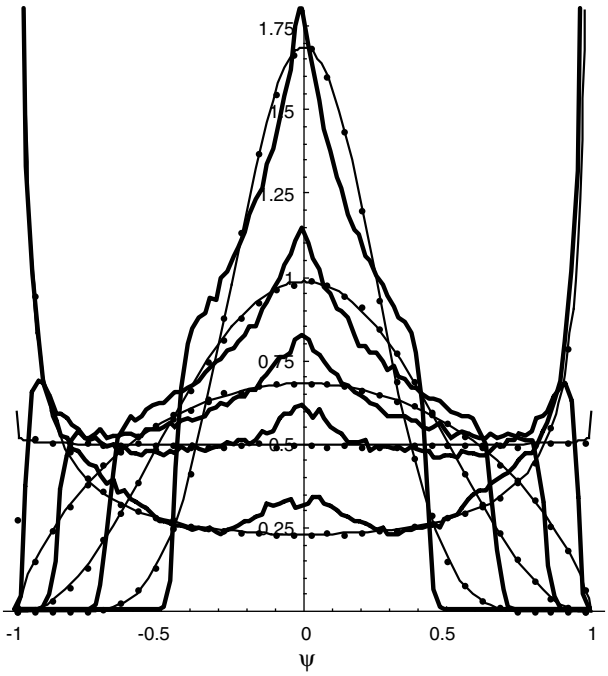

Fig. 2. Scalar PDF, $f(\psi;t)$, of an inert scalar evolving from an initial double-delta-function PDF; (•) MC particle model, (thick line) one-scalar EMST, (thin line) MC analytical solution (Eqs. (33) and (37) in [27]).

ansatz resulted in a close-to-Gaussian shaped PDF for the mean scalar gradient test case with two scalars. To avoid so-called stranding (Fig. 4 in [16]), i.e. the unphysical formation of pronounced branches in the EMST or the PDF, respectively, only a sub-ensemble of particles forms an EMST and participates in the mixing process during one time step. The particles in that sub-ensemble are selected from the whole ensemble in the grid cell by a random process (section 'Intermittency' in [16]). In the EMST mixing model, the mixing rate is actively controlled to match the exponential decay at high Reynolds numbers (section 'Determination of α' in [16]). In this work, the implementation by Ren, Subramaniam and Pope, downloaded from http://eccentric.mae.cornell.edu/tcg/emst/, was used as provided. This includes the intermittency parameters $Z_{0_l} = 1/6$, $Z_{0_u} = 1/6$, $Z_{1_l} = 0.0176$ and $Z_{1_u} = 0.3157$. As outlined in section 'Age Process Parameters' of [16], these choices were made based on numerical experimentation involving a mean scalar gradient test case. Here, Z_{0_l} and Z_{0_u} determine the range of the time intervals for which a particle is in the non-mixing state and Z_{1_l} and Z_{1_u} likewise for the mixing state. Correspondingly, the non-mixing intervals (horizontal sections of the EMST particle trajectory in Fig. 1) have all the same length ($Z_{0_l} = Z_{0_u}$), whereas the mixing intervals vary ($Z_{1_l} < Z_{1_u}$). In a small study based on the same test case as in the previous section, the EMST and MC models were compared for single-scalar mixing. The solutions of 10 simulations, each employing 20,000 particles, were averaged. The results are depicted in Fig. 2, where the different PDF stages obtained with the EMST and MC models share the same variance. After an initial transient phase, the last two PDF stages computed by the EMST model are more or less self-similar. This PDF shape, however, is not Gaussian as the one obtained with the MC model.

2.5. Parameterized scalar profile (PSP) mixing model

Similarly as in the development of the MC and EMST models, the basic ideas for the PSP mixing model [41,33] were first devised for one scalar. Later, its mathematical formulation could be extended for multiple scalars. Here, first the formulation of Meyer and Jenny [33] for homogeneous mixing problems is explained. The PSP model is constructed based on an idealization of the scalar distribution in high Reynolds number turbulent flows: an ensemble of one-dimensional scalar profiles is used to model the three-dimensional scalar field. The parameters that specify these profiles are assigned as additional properties to the computational particles. We assume that each fluid particle is convected for a certain time with one of these one-dimensional scalar profiles as depicted in Fig. 3. A reasonable approximation for the scalar distribution in such a profile is given by

$$\phi(x,t) = \exp\left(\frac{-t}{\tau_\phi^{(i)}}\right)\frac{\phi_+^{(i)} - \phi_-^{(i)}}{2}\sin\left(\frac{x\pi}{\lambda^{(i)}}\right) + \phi_c^{(i)}. \tag{14}$$

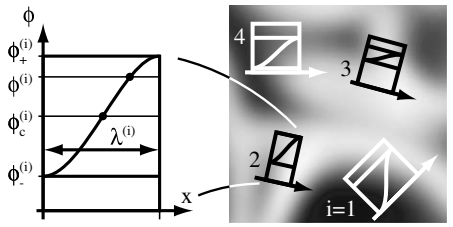

Fig. 3. Parameterized scalar profile of particle $i = 2$ and sketch of different profile realizations in a planar slice through a turbulent flow field (dark corresponds to a low scalar value).

In this relation, $\phi_c^{(i)} \equiv (\phi_+^{(i)} + \phi_-^{(i)})/2$ is the profile center on the scalar axis and x the local spatial profile coordinate. The profile was approximated by a sinusoidal shape that was parameterized by $\phi_-^{(i)}$, $\phi_+^{(i)}$, $\lambda^{(i)}$, and $\tau_\phi^{(i)}$. An alternative error-function based profile shape is discussed in Sections 2.1 (after Eq. (3)) and 3.3 (after Fig. 7) of [42]. Introducing this ansatz into the one-dimensional diffusion equation formulated in a Lagrangian reference frame for a fluid particle

$$\frac{\partial}{\partial t}\phi^{(i)} = \left(\Gamma \frac{\partial^2 \phi}{\partial x^2}\right)^{(i)}, \tag{15}$$

will lead to the expression $\lambda^{(i)} = \pi(\Gamma\tau_\phi^{(i)})^{1/2}$, which relates the mixing timescale $\tau_\phi^{(i)}$ with the profile lengthscale $\lambda^{(i)}$ and where Γ is the molecular diffusion coefficient. Modeling $\tau_\phi^{(i)}$ by using Spaldings suggestion, $\tau_\phi^{(i)} = 2/(C'_\phi \omega^{(i)})$, results in

$$\lambda^{(i)} = \pi\sqrt{\frac{2\Gamma}{C'_\phi \omega^{(i)}}}. \tag{16}$$

The scalar evolution of a particle can be obtained by using the ansatz (14) in the right-hand side of Eq. (15):

$$\frac{d\boldsymbol{\phi}^{(i)}}{dt} = -\frac{1}{2}C'_\phi \omega^{(i)}(\boldsymbol{\phi}^{(i)} - \boldsymbol{\phi}_c^{(i)}) \quad \text{with } \boldsymbol{\phi}_c^{(i)} \equiv \frac{\boldsymbol{\phi}_+^{(i)} + \boldsymbol{\phi}_-^{(i)}}{2}. \tag{17}$$

This is already the PSP model formulation for multiple scalars, which is a direct extension of the single-scalar form. Here, the scalar $\phi^{(i)}$ in the single-scalar form was replaced by the scalar vector $\boldsymbol{\phi}^{(i)} = (\phi_1, \phi_2, \ldots, \phi_{n_s})^T$. This expression is very similar to the IEM mixing model (Eq. (5)). In the IEM model, however, all profiles share the same lengthscale, $\lambda^{(i)} \propto \langle\omega\rangle^{-1/2}$, and the same profile center, $\phi_c^{(i)} = \langle\phi\rangle$. In that sense the PSP mixing model can be viewed as an extension of the IEM model. For joint PDF methods, which involve the turbulence frequency as a random variable, models for ω were developed. In this work, the gamma-distribution model by Jayesh and Pope (Section 12.5.3 in Pope [10]) is used. In a PDF method, the scalar PDF is described by an ensemble of particles. Since fluid particles at the profile boundaries are as well part of that ensemble, it is very natural to model the profile boundaries by representative particles from the ensemble, leading to a triplet which consists of the on-profile particle $\boldsymbol{\phi}^{(i)}$ and two particles representing the profile boundaries $\boldsymbol{\phi}_-^{(i)}$ and $\boldsymbol{\phi}_+^{(i)}$. The realizability condition

$$(\boldsymbol{\phi}^{(i)} - \boldsymbol{\phi}_-^{(i)}) \cdot (\boldsymbol{\phi}^{(i)} - \boldsymbol{\phi}_+^{(i)}) \leqslant 0, \tag{18}$$

which reduces in a the single-scalar case to $\phi_-^{(i)} \leqslant \phi^{(i)} \leqslant \phi_+^{(i)}$ (illustrated in Fig. 3) or $\phi_-^{(i)} \geqslant \phi^{(i)} \geqslant \phi_+^{(i)}$, ensures that the particle residing on a profile is enclosed by its profile boundaries $\phi_-^{(i)}$ and $\phi_+^{(i)}$. The boundary particles are chosen such that condition (18) is satisfied. To account for spatial decorrelation of a particle triplet, two intermittent aging processes $t_-^{(i)}$ and $t_+^{(i)}$ are used to reassign new boundary particles from time to time. Details about these processes and about the selection of boundary particles in a computationally efficient way are given in Section III B1 and Appendix A of [33], respectively. To honor mass conservation not only statistically for large particle ensembles but in every time step exactly, a correction scheme as outlined in Sections III B2 and 3 of [33] is employed.

Here, two different extensions of the PSP model for inhomogeneous mixing are presented. This involves multiple computational grid cells and unequally weighted particles. The particles in every grid cell represent the local PDF, which is assumed to have no spatial dependence within a grid cell. The computational grid needs to resolve spatial variations in the PDF. These variations take place on much larger scales, however, compared to the smallest scales present in certain realizations of the turbulent flow. So, based on the spatial homogeneity in one grid cell, the particles therein can be used to represent the local scalar fluctuations that are reduced by molecular mixing or by a mixing model. Using the previously outlined treatment of the particle boundaries in an inhomogeneous setting would imply consequently homogeneity over several grid cells. The reason is that particles belonging to one profile triplet can travel individually into different grid cells, which would enable the mixing of particles belonging to different grid cells. This is unfavorable since it reduces the effective spatial grid resolution. One possible remedy is to replace profile boundary representatives, which no longer belong to the same grid cell as the on-profile particle, by a similar particle of the same grid cell. More precisely, the nearest neighbor in scalar space has to be found. Note that this requires looping over all particles of the ensemble (same cell) and therefore comes at a certain price. We will refer to the boundary treatment just outlined as nearest neighbor approach.

In the implementation described so far, the dynamics of the profile boundary and on-profile particles are very similar, since the profile boundaries have for subsequent time intervals the same trajectories as different on-profile particles. In a second approach, the profile boundary values, which are still assigned as outlined before, evolve according to

$$\frac{d\boldsymbol{\phi}_{\pm}^{(i)}}{dt} = -\frac{1}{2}C_{\phi}''\langle\omega\rangle(\boldsymbol{\phi}_{\pm}^{(i)} - \langle\boldsymbol{\phi}\rangle), \tag{19}$$

where C_{ϕ}'' is an additional model constant to be determined. Note that the evolution of the profile boundaries, $\boldsymbol{\phi}_{+}^{(i)}$ and $\boldsymbol{\phi}_{-}^{(i)}$, are no longer described by the evolution of other notional particles like in the nearest neighbor approach, but are additional properties of particle i, which change according to the deterministic IEM-like model (19) and the already mentioned aging processes $t_{-}^{(i)}$ and $t_{+}^{(i)}$. Consequently, since particles are no longer linked to each other through particle triplets, the computationally expensive search for nearest neighbors in scalar space is no longer required when particles cross cell boundaries. For the numerical time integration of Eqs. (17) and (19), the same scheme (7) as for the IEM mixing model is used.

Depending on the PDF solution algorithm, different particle weights may be used. In that case, the probability of selecting particle i at the beginning of a profile-boundary life cycle has to be proportional to its weight $w^{(i)}$. This is achieved by the following algorithm: in Fig. 4a, the axis is partitioned into n_p (e.g. $n_p = 5$) different sections, where the length of the ith section is proportional to the particle weight $w^{(i)}$. The particle i is selected if the equally distributed random variable $v \in [0,1]$ fulfills

$$\sum_{j=1}^{i-1}\frac{w^{(j)}}{W} < v \leqslant \sum_{j=1}^{i}\frac{w^{(j)}}{W},$$

where W is the sum of the individual particle weights (definition (4)). Finding the corresponding interval on the v-axis can most simply be achieved by a linear search. Depending on the time-step size to boundary-renewal-timescale ratio, in each time step a certain fraction of profile boundaries has to be updated. Therefore, the computational cost of the outlined algorithm becomes proportional to n_p^2. However, the particle selection can be done more efficiently as described next: at the beginning of each time step, n_p bins of equal size $1/n_p$ are created as depicted in Fig. 4b. The particle with index i is added to the bin k if

$$\left[\sum_{j=1}^{i-1}\frac{w^{(j)}}{W}, \sum_{j=1}^{i}\frac{w^{(j)}}{W}\right] \cap \left[\frac{k-1}{n_p}, \frac{k}{n_p}\right] \neq 0.$$

By using $k = \text{ceiling}(vn_p)$ to identify a certain bin, the number of candidates is reduced drastically and therefore a possible subsequent linear search within one bin becomes a much cheaper operation. A numerical experiment with uniformly distributed particle weights $w^{(i)} \in (0,1]$ confirmed that the scaling is reduced to approximately n_p.

3. Mixing model validation

In this section, the evolution of the joint scalar PDF predicted by various mixing models is assessed. In order to focus on the effects of molecular mixing in isolation, no chemical reactions are considered for the following computational studies. Furthermore, note that convective scalar transport is closed in joint velocity–composition PDF methods, which facilitates simple benchmark configurations.

3.1. Spatially inhomogeneous two-scalar mixing

3.1.1. Governing equations and numerical method

As a first test case, the so-called three-stream problem, recommended by Klimenko and Pope [30] for model validation, is considered. The DNS reference data is provided by Juneja and Pope [7]. It involves two inert scalars that mix in a stationary homogeneous turbulent flow. The corresponding simplified form of the PDF transport Eq. (3) is

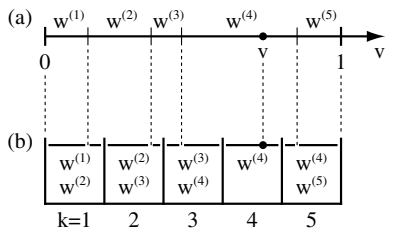

Fig. 4. Random selection from a set of unequally likely events $w^{(i)}$; (a) uniformly distributed random selector variable v, (b) lookup table for the efficient event selection in the form of a set of equally sized bins.

$$\frac{\partial f}{\partial t} = -\frac{\partial}{\partial \psi_\alpha}\left(f\langle \Gamma_{(\alpha)}\nabla^2\phi'_\alpha|\boldsymbol{\psi}\rangle\right), \tag{20}$$

where $f(\boldsymbol{\psi};\mathbf{x},t)$ is the joint scalar PDF (Eq. (2) in [7] or Eq. (12.345) in [10]). Juneja and Pope report that the evolution from the initial two-scalar PDF is fairly independent of the Reynolds number. For their DNS they chose a Prandtl number of $Pr = 0.7$ and the Taylor-scale Reynolds number was $Re_\lambda = 48.6$ and 92.4. To validate the suggested algorithmic extensions of the PSP model for inhomogeneous mixing, a constant flow velocity $\mathbf{U} = (U,0,0)^T$ was added to the three-dimensional mixing scenario investigated by Juneja and Pope. The corresponding joint velocity–composition–turbulence frequency PDF is $f(\mathbf{V},\boldsymbol{\psi},\theta;\mathbf{x},t) = \delta(\mathbf{V}-\mathbf{U})f(\boldsymbol{\psi},\theta;x,t)$, where θ is the sample space coordinate of the instantaneous turbulence frequency ω and $\mathbf{x} = (x,0,0)^T$ was used. Introducing this PDF into the transport Eq. (3) augmented by the transport term for the turbulence frequency will lead after integration over velocity sample space $\mathbf{V}$ to

$$\frac{\partial f}{\partial t} + U\frac{\partial f}{\partial x} = -\frac{\partial}{\partial \psi_\alpha}\left(f\langle \Gamma_{(\alpha)}\nabla^2\phi'_\alpha|\boldsymbol{\psi},\theta\rangle\right) - \frac{\partial}{\partial\theta}\left(f\left\langle\frac{\mathrm{D}\omega}{\mathrm{D}t}\middle|\boldsymbol{\psi},\theta\right\rangle\right). \tag{21}$$

This equation describes the evolution of the Eulerian composition–frequency joint PDF $f(\boldsymbol{\psi},\theta;x,t)$ as a function of the downstream coordinate x. In a reference frame moving with the flow velocity U in downstream direction, the problem reduces to the one solved in the DNS ($\mathrm{D}f/\mathrm{D}t = \partial f/\partial t + U\partial f/\partial x$). Likewise, the initial condition of the DNS transforms into an inflow boundary condition. To summarize in more application oriented terms, a batch reactor was replaced by a plug-flow reactor. For our purpose the resulting problem is ideally suited since it is spatially inhomogeneous, challenging with respect to molecular mixing and well documented (DNS data). From the connections between Eulerian and Lagrangian PDFs (Chapter 12.2.5 in [10]), and between Fokker–Planck and Langevin equations (Chapter 4.3.5 in [43]) one obtains the stochastic differential equations (SDEs)

$$\begin{aligned} dx^{(i)} &= U\,dt,\\ d\phi_\alpha^{(i)} &= \mathrm{M}(\{\boldsymbol{\phi}'\},\{\omega\})dt \text{ and}\\ d\omega^{(i)} &= -(\omega^{(i)} - \langle\omega\rangle)\frac{dt}{T_\omega} + \sqrt{\frac{2\sigma^2\langle\omega\rangle\omega^{(i)}}{T_\omega}}dW. \end{aligned} \tag{22}$$

The mixing model contribution is given by $\mathrm{M}(\{\boldsymbol{\phi}'\},\{\omega\})$, where $\{\boldsymbol{\phi}'\}$ and $\{\omega\}$ are used to represent the fluctuating scalar vectors and turbulence frequency values of the particle ensemble in one grid cell. The third equation is the stationary form of the gamma-distribution model suggested by Jayesh and Pope (Eq. (12.191) in [10]). Note that this model provides a turbulence timescale, which is required for joint velocity–composition PDF methods. The timescale $T_\omega \equiv 1/(C_3\langle\omega\rangle)$ involves the model constant C_3, σ^2 is the variance of $\omega^{(i)}/\langle\omega\rangle$ and $W(t)$ is a Wiener process.

An ensemble of particles, representing the PDF $f(\boldsymbol{\psi},\theta;x,t)$, can now be evolved according to the Eq. (22). Therefore, the computer program by Meyer and Jenny [44] was used. This code solves the joint velocity–turbulence frequency PDF transport equation on a one-dimensional solution domain. In the present work, the SDEs for the scalar evolution including the different mixing models were added. In order to match the initial condition of the DNS at the inflow boundary, the spectral procedure used for the initialization of the DNS by Juneja and Pope [7] (Section III) was used. As a result one obtains an ensemble of grid points that contain not only the scalar values but also their spatial gradients. To match the scalar PDF, these points are directly used for the initialization of the stochastic particles. Different than other mixing models, however, the PSP model can as well use the gradient information for the selection of the initial scalar-profile parameters. Here, for every particle a search for the profile parameters, which reproduce the DNS gradient data most accurately, is performed. Consequently, the joint scalar–scalar gradient statistics at the inflow boundary can be honored by the PSP model. Further details are available in section IV B of [33]. To estimate statistical quantities, e.g. $\langle\omega\rangle$, the x-axis is partitioned into 100 equally sized grid cells, where on average 100 particles per grid cell were employed. In each grid cell, the joint composition PDF is estimated by a histogram using 60×60 bins. To obtain smooth scalar PDFs, time averaging was applied. A domain length of $2U/\langle\omega\rangle$ was used together with a time step $\Delta t = 0.001/\langle\omega\rangle$ and the standard frequency model parameters $C_3 = 1$ and $\sigma^2 = 1/4$. For the PSP nearest neighbor version, the parameters $C'_\phi = 13$ and $C_t = 0.15C'_\phi$ for the boundary aging process provided the correct high-Reynolds-number scalar variance decay rate and the best agreement with the DNS, while for the PSP version with IEM boundary treatment (PSP IEM) $C'_\phi = 13$, $C''_\phi = 0.1C'_\phi$ and $C_t = C'_\phi$ are appropriate.

3.1.2. Discussion results

In Fig. 5, the rms value of scalar 1, $\phi''_1(x)$, is plotted as a function of the downstream coordinate x. It can be seen that the IEM, CD, MCD and EMST predict a constant decay rate. As already mentioned in Section 2.4, for the EMST model this is so by construction. The IEM model is calibrated to reproduce the correct constant decay rate (Eq. (6) in Section 2.1) that is observed in turbulent flows with a scalar energy spectrum in equilibrium (Fig. 12 in [7]). For the Curl models it is shown in the appendix that consistent decay rates are achieved with appropriately selected C'_ϕ. As soon as a self-similar PDF shape is attained, also the PSP model predicts a consistent decay rate, which is analogous to the MC as discussed in Section 2.3. In principle, this is in agreement with DNS observations (Fig. 10 in [28]), where the scalar energy spectrum has to equilibrate first before a constant decay rate is attained. In Figs. 6 and 7, the joint scalar PDF $f(\boldsymbol{\psi};x)$ provided by the different mixing

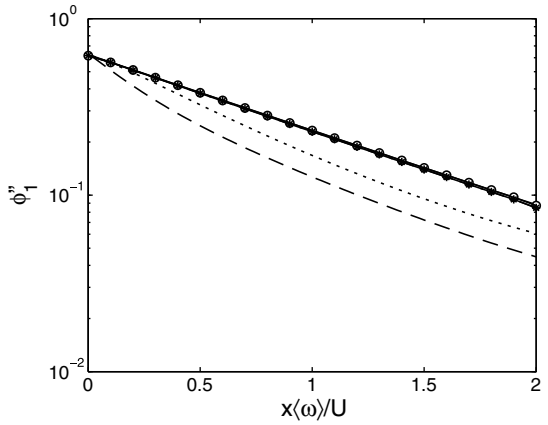

Fig. 5. Rms decay of scalar 1, $\phi''_1(x)$, in downstream direction x; (○) IEM, (dash dot line) CD, (∗) MCD, (solid line) EMST, (dashed line) PSP IEM, (dotted line) PSP nearest neighbor. The curves of the IEM, CD, MCD and EMST models overlap.

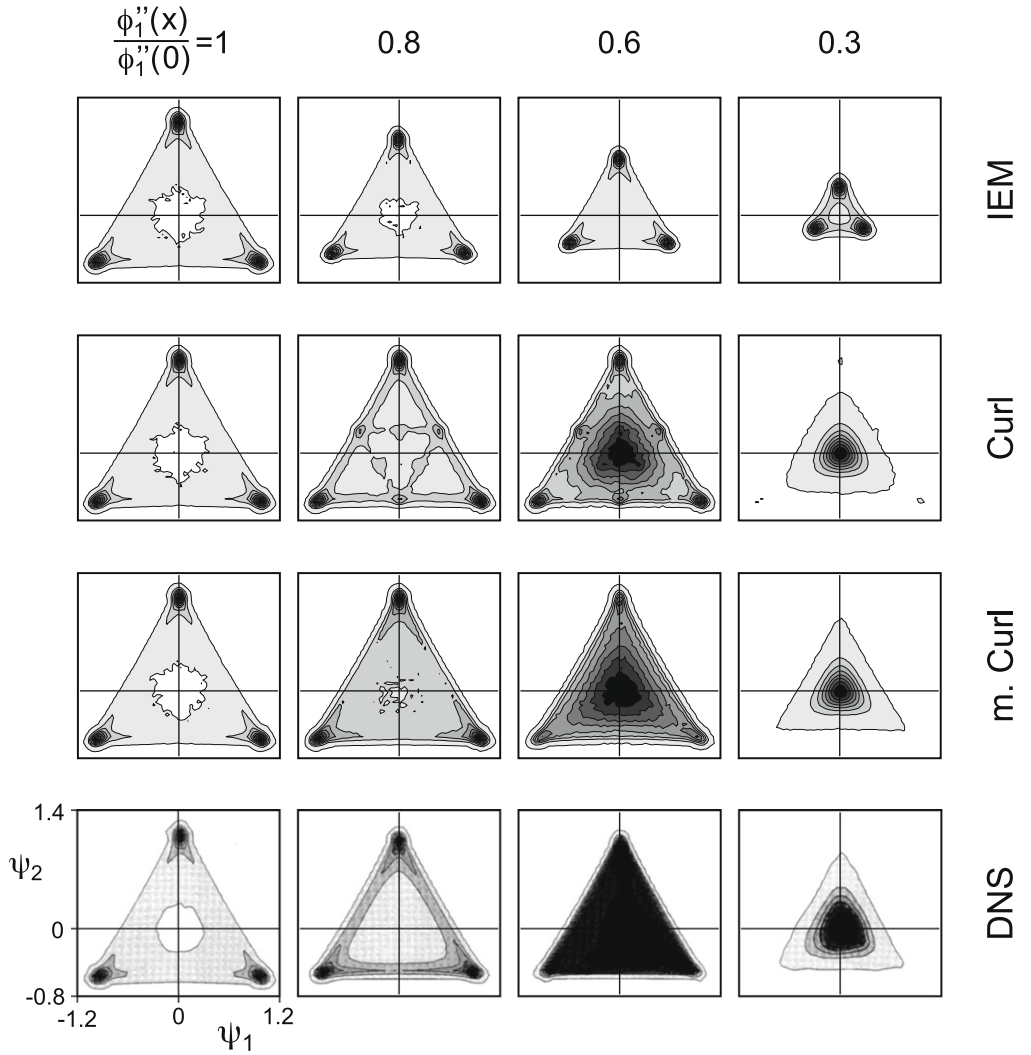

Fig. 6. Evolution of the joint composition PDF $f(\boldsymbol{\psi};x)$ with $\boldsymbol{\psi}=(\psi_1,\psi_2)^T$, mixing model set 1; rows correspond to different mixing models and the reference DNS R92A by Juneja and Pope [7], and columns to different normalized rms values $\phi''_1(x)/\phi''_1(0)$; the 10 contour levels range from 0.01 to 1 (black) and represent the PDF normalized by its maximum value.

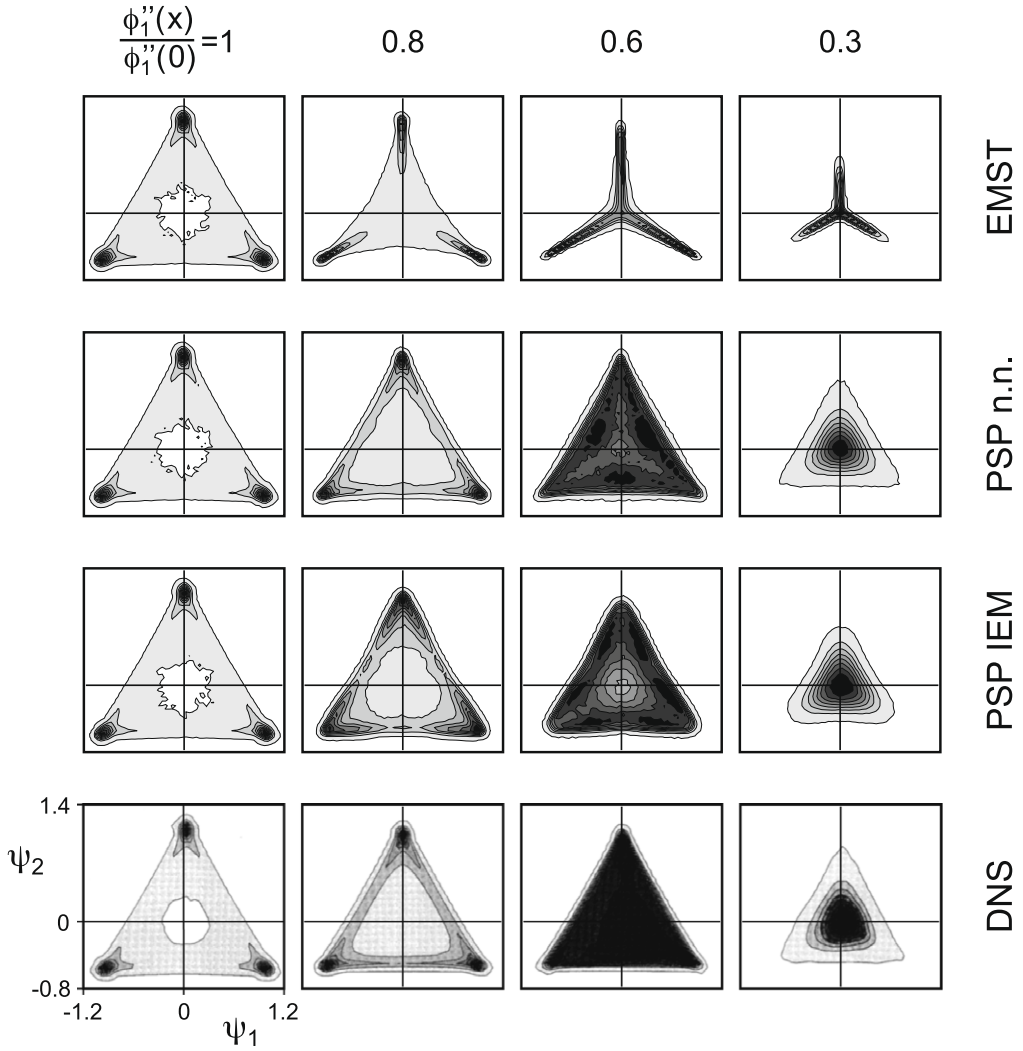

Fig. 7. Evolution of the joint composition PDF $f(\boldsymbol{\psi};x)$ with $\boldsymbol{\psi} = (\psi_1, \psi_2)^T$, mixing model set 2; same as Fig. 6.

models are compared with the DNS case R92A of Juneja and Pope [7] for different normalized root mean square (rms) values of scalar 1. Essentially three different mixtures, represented by the peaks in the histograms of the first column in Figs. 6 and 7, are present initially. Later three different characteristic PDF stages are observed in the DNS: first diffusion starts at the interfaces of the more or less pure mixture pockets and consequently, the peaks smear out along their connecting lines, then a uniform triangular-shaped PDF forms and finally the PDF approaches a bi-variate Gaussian PDF. Based on the excellent results of the PSP formulation for homogeneous cases [33], the good performance of the PSP nearest neighbor model is not surprising. The agreement of the results from the PSP IEM model is slightly worse but still satisfactory. Also in good agreement with the DNS are the results from the conceptually simple Curl models. Although the PDFs of the CD model contain some pronounced artifacts originating from the nature of the model (pairing of particles from different peaks), the CD and the MCD models are able to predict the basic PDF evolution stages fairly accurately. The poor performance of the IEM model is due to the shape preserving property, which was already pointed out in Section 2.1. The predictions of the EMST mixing model are not satisfactory either. Global branches are formed although the recommended intermittency parameters were used. More insight to understand this behavior can be gained from Fig. 8. An ensemble of 1000 particles was initialized according to a bi-variate standard normal distribution in scalar space. Shown are the particles after 10 EMST time steps with $\Delta t = 0.01/\langle\omega\rangle$. In an inhomogeneous mixing scenario, this problem may be less dramatic since particle transport in physical space counteracts stranding, which occurs in individual computational grid cells. However, the quantification of this effect is problem-dependent. Alternatively, the parameters of the intermittency process could be adjusted. This is feasible within a limited range as discussed in section 'Age Process Parameters' of [16]. Decreasing Z_{1_l} and Z_{1_u}, however, reduces the number of particles in the mixing sub-ensemble and consequently weakens localness with respect to the entire ensemble in scalar space.

Fig. 8. Particles evolved from a joint standard normal distribution in scalar space using the EMST mixing model; (•) mixing particles which are part of the EMST, (○) non-mixing particles.

Formally, this is an extension of the single-scalar test case to a virtually arbitrary number of scalars. As already mentioned near the end of Section 1.2, the mixing models M considered in this work do not depend on velocity.

In a number of numerical experiments, the previously outlined particle evolution equations were solved for different particle ensembles. Here, the influence of the mixing model, the number of scalars n_s and the number of particles n_p on the scalar statistics and on the computational cost was investigated. The same mixing and frequency model parameters as in Section 3.1 were used and the SLM model constant C_0 was 2.1. The reference for comparison is the DNS 'Run 256.5' by Overholt and Pope [5], for which $Re_\lambda = 185$, $\beta = 1m^{-1}$, $k = 577\frac{m^2}{s^2}$, the turbulent dissipation $\varepsilon = 2641\frac{J}{kg\,s}$ and the eddy turnover time $T_E = 0.07028$ s. From these quantities one obtains the mean turbulence frequency $\langle\omega\rangle \equiv \varepsilon/k = 4.577\ \mathrm{s}^{-1}$ and integral turbulence lengthscale $L \equiv (2k/3)^{3/2}/\varepsilon = 2.857$ m. The same simulation framework as for the previous section was used with a time-step size of $\Delta t = 0.02T_E$. At the beginning of each simulation the scalar fluctuations $\boldsymbol{\phi}'^{(i)}$ were set to 0. The velocities $\boldsymbol{U}^{(i)}$ and turbulence frequencies $\omega^{(i)}$ on the other hand were initialized with suitable random number generators. After a statistically stationary state was reached, time averaging was applied to improve scalar statistics. Note that for this test case the statistics of the individual scalars are identical and therefore can be averaged to further reduce the statistical error of the results. To quantify the statistical error of the averaged statistics, 95%-confidence intervals were used. Here, the standard deviation of the statistically dependent samples were estimated by a standard AR(p) time series model [45]. Simulations with varying n_s and constant $n_p = 2^9 = 512$, and calculations with two scalars and variable number of particles were carried out.

3.2.2. Discussion results

In Figs. 9 and 11, the normalized scalar variance and kurtosis are plotted as functions of n_s. Here, the violation of the independence and linearity requirement by the EMST and PSP mixing models manifests itself through the dependence on n_s. This is not the case for the other models since each scalar is treated independently. For large n_s, the EMST results approach those

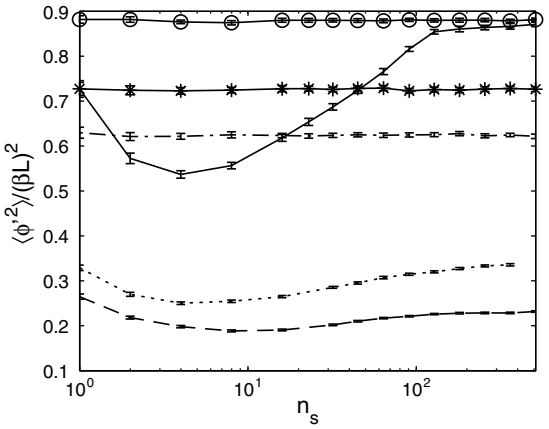

Fig. 9. Non-dimensional scalar variance, $\langle\phi'^2\rangle/(\beta L)^2$, as function of the number of scalars n_s; (○) IEM, (dash dot line) CD, (∗) MCD, (solid line) EMST, (dashed line) PSP IEM, (dotted line) PSP nearest neighbor.

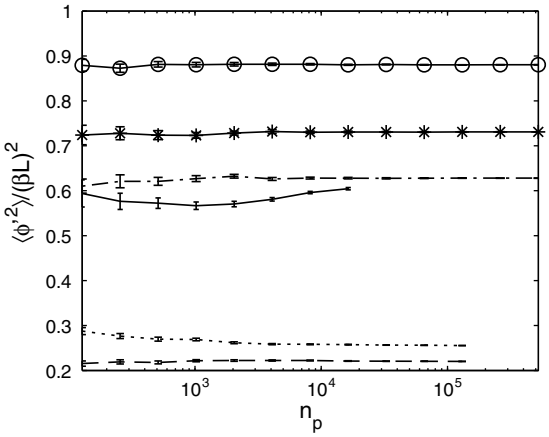

Fig. 10. Non-dimensional scalar variance, $\langle\phi'^2\rangle/(\beta L)^2$, as function of the number of particles n_p; same as Fig. 9.

of the IEM model, while the predictions of the PSP mixing models are closest to the equilibrium variance $\langle \phi'^2 \rangle = 0.3052(\beta L)^2$ obtained with the DNS (Table II in [5]). The IEM mixing model predicts a kurtosis of 3, which corresponds to a Gaussian distribution. This is not surprising: with the IEM model (Eq. (5)) substituted for M in Eq. (26) one obtains an Ornstein–Uhlenbeck process (Eq. (J.39) in [10]) for which the stationary solution is a Gaussian PDF. As already mentioned in Section 2.4, the

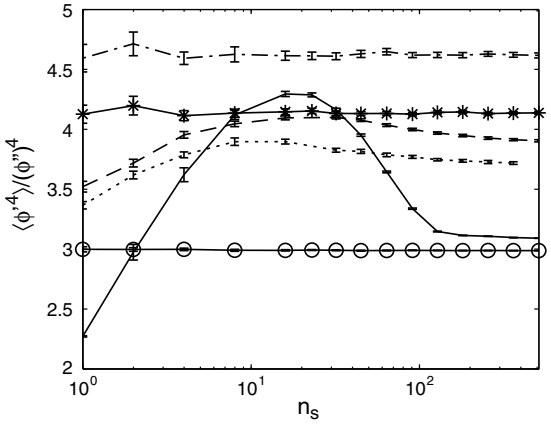

Fig. 11. Scalar kurtosis as function of the number of scalars n_s; same as Fig. 9.

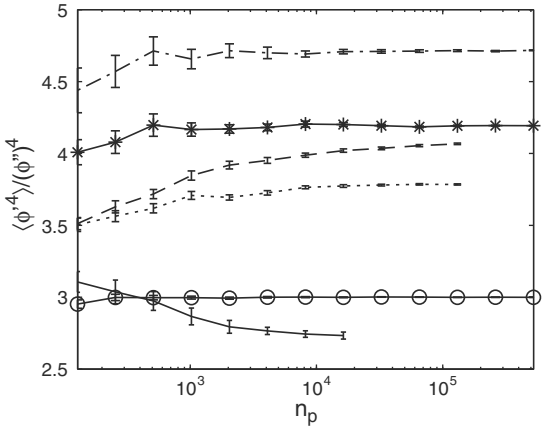

Fig. 12. Scalar kurtosis as function of the number of particles n_p; same as Fig. 9.

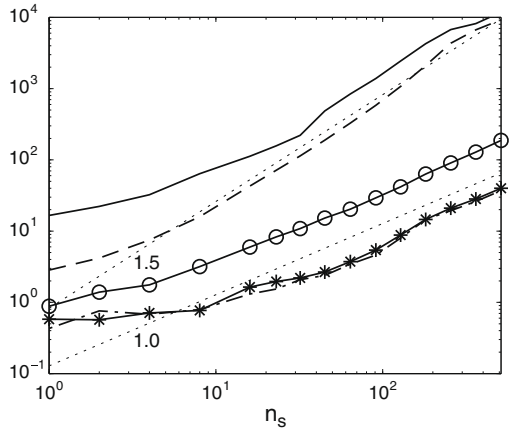

Fig. 13. Computational cost (CPU-time in seconds) as function of the number of scalars n_s; (○) IEM, (dash dot line) CD, (∗) MCD, (solid line) EMST, (dashed line) PSP IEM, (dotted lines) power laws with indicated exponents.

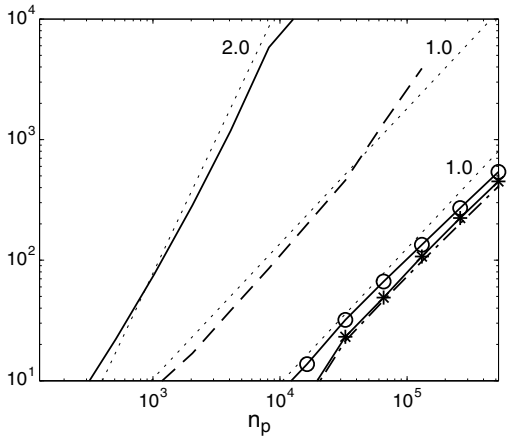

Fig. 14. Computational cost (CPU-time in seconds) as function of the number of particles n_p; same as Fig. 13.

exact agreement of the kurtosis predicted by the EMST model for $n_s = 2$ is resulting from the choice of the contraction coefficient. In Figs. 10 and 12 it can be observed that the dependence of the scalar statistics on the number of particles n_p is rather weak. The variance $\langle \phi'^2 \rangle = 0.599(\beta L)^2$ found for the EMST model with $n_p = 2^{13} = 8192$ is consistent with the value reported by Subramaniam and Pope (Table 4 in [16]).

Fig. 13 shows the dependence of the computational costs on n_s. For the EMST model, a linear dependency can be observed for $n_s < 30$. Once n_s exceeds 30, the computational cost becomes proportional to $n_s^{1.5}$ similar as for the PSP IEM model. The most expensive component in the PSP IEM model is the mass conservation algorithm mentioned in Section 2.5. The computational costs of the Curl models and the IEM model scale linearly with n_s. As shown in Fig. 14 the computational costs for the CD, MCD, IEM and PSP IEM mixing models scale approximately linearly with n_p while a close to quadratic dependence can be observed for the EMST model. The PSP nearest neighbor version was not considered in this study since its computational cost is substantially lower for homogeneous cases involving just one grid cell compared to inhomogeneous settings (Section 2.5).

4. Conclusions

Mixing models are required for the closure of the molecular diffusion term in PDF and FDF methods. In the present study, the performance of two new PSP model versions was assessed and compared with some of the most widely used mixing models. The test cases, which focus on the accurate prediction of molecular mixing, include an inhomogeneous mixing scenario, where the evolution of a joint two-scalar PDF was considered, and multi-scalar mixing involving mean scalar gradients. The CD, MCD and IEM models are computationally very efficient; i.e. their cost scales linearly with the number of scalars and particles. If the dynamics of inert scalars have to be predicted or spatially distributed chemical reactions are treated, and consequently localness is less important, the MCD model provides accurate results at low cost. The PSP mixing model was successfully extended for inhomogeneous flows and provides very accurate results at reasonable computational cost. Unlike the Curl models, the particle trajectories computed by the PSP models are continuous in scalar space over time and the weak localness criterion is fulfilled. Consequently, the mixing of reactants over localized flame fronts without reaction is inhibited. The EMST mixing model comes closest to being local in a strong sense, however, it is rather expensive and the formation of branches in scalar space, so-called stranding, remains an issue. An open point for future research is the performance of the PSP model in reacting flows.

Acknowledgment

This work was financially supported by the Swiss National Science Foundation.

Appendix A. Model constants in Curl models

In this section, for simplicity the derivations are made for a single-scalar case but extend straightforwardly to multiple scalars, since different scalars are treated independently in Curl's models. Starting from Eq. (187) of [18], written in a notation consistent with this paper,

$$\frac{\partial f(\psi;t)}{\partial t} = 2C'_\phi \langle \omega \rangle \int\int [f(\psi_\circ;t) f(\psi_\bullet;t) f(\psi|\psi_\circ,\psi_\bullet) - f(\psi;t)] d\psi_\circ d\psi_\bullet, \tag{A.1}$$

where $f(\psi|\psi_\circ,\psi_\bullet)$ is a transition probability from given $\psi_\circ$ and $\psi_\bullet$ to ψ, and C'_ϕ is a model constant similar to C_ϕ in Eq. (5). With the transition probability

$$f(\psi|\psi_\circ,\psi_\bullet) \equiv \delta\left(\psi - \frac{\psi_\circ+\psi_\bullet}{2}\right),$$

corresponding to Curl's CD model, the evolution of the variance can be expressed as

$$\begin{aligned}\frac{\partial\langle\phi^2\rangle}{\partial t} &= 2C'_\phi\langle\omega\rangle\int\int\int\psi^2\left[f(\psi_\circ;t)f(\psi_\bullet;t)\delta\left(\psi-\frac{\psi_\circ+\psi_\bullet}{2}\right)-f(\psi;t)\right]d\psi_\circ d\psi_\bullet d\psi\\ &= 2C'_\phi\langle\omega\rangle\int\int\left[f(\psi_\circ;t)f(\psi_\bullet;t)\left(\frac{\psi_\circ+\psi_\bullet}{2}\right)^2\right]d\psi_\circ d\psi_\bullet - \langle\phi^2\rangle\\ &= 2C'_\phi\langle\omega\rangle\left[\frac{1}{4}(\langle\phi^2\rangle+2\langle\phi\rangle^2+\langle\phi^2\rangle)-\langle\phi^2\rangle\right]\\ \frac{d}{dt}\ln\langle\phi'^2\rangle &= -C'_\phi\langle\omega\rangle. \end{aligned} \tag{A.2}$$

Here, in the second step the sifting property of the δ-function and in the last step $\langle\phi\rangle\neq\langle\phi\rangle(t)$ were used. Performing the same steps for the transition probability of the MCD model,

$$f(\psi|\psi_\circ,\psi_\bullet) \equiv \begin{cases}\frac{1}{\psi_\circ-\psi_\bullet} & \text{if } \psi_\circ\leqslant\psi\leqslant\psi_\bullet\\ 0 & \text{else,}\end{cases} \tag{A.3}$$

one obtains

$$\frac{d}{dt}\ln\langle\phi'^2\rangle = -\frac{2}{3}C'_\phi\langle\omega\rangle. \tag{A.4}$$

Comparing the variance decay rates of the Curl models, Eqs. (A.2) and (A.4), with the one of the IEM, Eq. (6), we get the same decay rate for the CD model with $C'_\phi=2$ but for the MCD $C'_\phi=3$ should be used.

The variance decay rate can as well be determined from the stochastic differential equations of the notional particles. The resulting Eq. (193) in [18], based on equally weighted particles, is

$$\frac{1}{\langle\phi'^2\rangle^q}\frac{\langle\phi'^2\rangle^{q+1}-\langle\phi'^2\rangle^q}{\Delta t} = -\frac{n_m}{2n_p\Delta t} \tag{A.5}$$

for Curl's CD model. Here, q is the time-step index, Δt the time-step size, n_m the number of mixing particles, and n_p the overall number of particles. Comparing this with Eq. (A.2) leads to the relation

$$n_m = 2C'_\phi n_p\Delta t\langle\omega\rangle. \tag{A.6}$$

Based on the mixing mechanism of the modified Curl model,

$$\begin{aligned}\phi_\circ^{(j)q+1} &= \phi_\circ^{(j)q} + h^{(j)}(\phi_\bullet^{(j)q}-\phi_\circ^{(j)q})\\ \phi_\bullet^{(j)q+1} &= \phi_\bullet^{(j)q} + h^{(j)}(\phi_\circ^{(j)q}-\phi_\bullet^{(j)q})\end{aligned} \tag{A.7}$$

given for the particle pair j and starting from

$$\langle\phi^2\rangle^{q+1} = \frac{1}{n_p}\sum_{i=1}^{n_p}(\phi^{(i)q+1})^2, \tag{A.8}$$

which is valid for large n_p, an equation similar to expression (A.5) can be derived: note that the formulation (A.7) is in accordance with the transition probability (A.3) but distinctly different compared to Eq. (9). For equally weighted particles both forms are statistically equivalent. Decomposing the sum in Eq. (A.8) into n_m mixing and n_p-n_m non-mixing particles,

$$\langle\phi^2\rangle^{q+1} = \frac{1}{n_p}\left[\sum_{i=1}^{n_m}(\phi^{(i)q+1})^2 + \sum_{i=n_m+1}^{n_p}(\phi^{(i)q})^2\right], \tag{A.9}$$

one can set the second sum equal to $(n_p-n_m)\langle\phi^2\rangle^q$ and write the first term as a sum over particle pairs:

$$\sum_{i=1}^{n_m}(\phi^{(i)q+1})^2 = \sum_{j=1}^{n_m/2}\left[(\phi_\circ^{(j)q+1})^2+(\phi_\bullet^{(j)q+1})^2\right]. \tag{A.10}$$

Combining this with the mixing mechanism (A.7) and having the $h^{(j)}$, $\phi_\circ^{(j)q}$ and $\phi_\bullet^{(j)q}$ selected statistically independently of each other, one can simplify the resulting expression to

$$\sum_{i=1}^{n_m}(\phi^{(i)q+1})^2 = n_m\left[\langle\phi^2\rangle^q + \frac{2}{3}(\langle\phi^2\rangle^q - \langle\phi\rangle^{2q})\right]. \tag{A.11}$$

Here, for $h^{(j)} \in [0,1]$ we used $\langle h\rangle = 1/2$ and $\langle h^2\rangle = 1/3$. Inserting these results together with $\langle\phi\rangle^{2q+1} = \langle\phi\rangle^{2q}$ and $\langle\phi'^2\rangle = \langle\phi^2\rangle - \langle\phi\rangle^2$ in Eq. (A.9) leads to

$$\frac{1}{\langle\phi'^2\rangle^q}\frac{\langle\phi'^2\rangle^{q+1} - \langle\phi'^2\rangle^q}{\Delta t} = -\frac{n_m}{3n_p\Delta t}. \tag{A.12}$$

Eq. (A.7) with $h^{(j)} \in [0,1/2]$ is equivalent to expression (9) for equally weighted particles. As already claimed, this leads together with $\langle h\rangle = 1/4$ and $\langle h^2\rangle = 1/12$ as well to Eq. (A.11) and finally to Eq. (A.12). Note however that for non-equally weighted particles a mass conserving formulation similar to Eq. (A.7) with $h^{(j)} \in [0,1]$ is violating boundedness in scalar space, whereas expression (10) remains bounded. Finally, comparing Eq. (A.12) with Eq. (A.4) gives for the modified Curl as for the original Curl model the relation (A.6).

References

[1] Z. Warhaft, Passive scalars in turbulent flows, Annual Review of Fluid Mechanics 32 (2000) 203–240.
[2] B.I. Shraiman, E.D. Siggia, Scalar turbulence, Nature 405 (6787) (2000) 639–646.
[3] R.O. Fox, Computational Models for Turbulent Reacting Flows, Cambridge University Press, Cambridge, 2003.
[4] S.B. Pope, The vanishing effect of molecular diffusivity on turbulent dispersion: implications for turbulent mixing and the scalar flux, Journal of Fluid Mechanics 359 (1998) 299–312.
[5] M.R. Overholt, S.B. Pope, Direct numerical simulation of a passive scalar with imposed mean gradient in isotropic turbulence, Physics of Fluids 8 (11) (1996) 3128–3148.
[6] P.K. Yeung, S.B. Pope, Differential diffusion of passive scalars in isotropic turbulence, Physics of Fluids a-Fluid Dynamics 5 (10) (1993) 2467–2478.
[7] A. Juneja, S.B. Pope, A DNS study of turbulent mixing of two passive scalars, Physics of Fluids 8 (8) (1996) 2161–2184.
[8] S.B. Pope, Pdf methods for turbulent reactive flows, Progress in Energy and Combustion Science 11 (2) (1985) 119–192.
[9] S.B. Pope, Lagrangian PDF methods for turbulent flows, Annual Review of Fluid Mechanics 26 (1994) 23–63.
[10] S.B. Pope, Turbulent Flows, Cambridge University Press, Cambridge, 2000.
[11] A.R. Kerstein, A linear-eddy model of turbulent scalar transport and mixing, Combustion Science and Technology 60 (4-6) (1988) 391–421.
[12] P.J. Colucci, F.A. Jaberi, P. Givi, S.B. Pope, Filtered density function for large eddy simulation of turbulent reacting flows, Physics of Fluids 10 (2) (1998) 499–515.
[13] V. Raman, H. Pitsch, R.O. Fox, Hybrid large-eddy simulation/lagrangian filtered-density-function approach for simulating turbulent combustion, Combustion and Flame 143 (1-2) (2005) 56–78.
[14] V. Raman, H. Pitsch, A consistent les/filtered-density function formulation for the simulation of turbulent flames with detailed chemistry, Proceedings of the Combustion Institute 31 (2) (2007) 1711–1719.
[15] S.B. Pope, Advances in PDF methods for turbulent reactive flows, in: H.I. Andersson, P.A. Krogstad (Eds.), Tenth European Turbulence Conference, CIMNE, Trondheim, 2004, pp. 529–536.
[16] S. Subramaniam, S.B. Pope, A mixing model for turbulent reactive flows based on euclidean minimum spanning trees, Combustion and Flame 115 (4) (1998) 487–514.
[17] R.L. Curl, Dispersed phase mixing: 1. theory and effects in simple reactors, Aiche Journal 9 (2) (1963) 175–181.
[18] C. Dopazo, Recent developments in PDF methods, in: P.A. Libby, F.A. Williams (Eds.), Turbulent Reacting Flows, Academic Press, London etc., 1994, pp. 375–474.
[19] J. Janicka, W. Kolbe, W. Kollmann, Closure of the transport-equation for the probability density-function of turbulent scalar fields, Journal of Non-Equilibrium Thermodynamics 4 (1) (1979) 47–66.
[20] A.T. Norris, S.B. Pope, Modeling of extinction in turbulent-diffusion flames by the velocity-dissipation-composition PDF method, Combustion and Flame 100 (1-2) (1995) 211–220.
[21] J. Villermaux, J.C. Devillon, Representation de la coalescence et de la redispersion des domaines de segregation dans un fluide par un modele d'interaction phenomenologique, in: Second International Symposium on Chemical Reaction Engineering, Elsevier, New York, 1972, pp. 1–13.
[22] C. Dopazo, E.E. Obrien, Approach to autoignition of a turbulent mixture, Acta Astronautica 1 (9-10) (1974) 1239–1266.
[23] J.M. Ottino, The Kinematics of Mixing: Stretching, Chaos, and Transport, Cambridge University Press, Cambridge, 1989.
[24] R.O. Fox, The Fokker–Planck closure for turbulent molecular mixing – passive scalars, Physics of Fluids 4 (6) (1992) 1230–1244.
[25] R.O. Fox, Improved Fokker–Planck model for the joint scalar, scalar gradient PDF, Physics of Fluids 6 (1) (1994) 334–348.
[26] R.O. Fox, P.K. Yeung, Improved lagrangian mixing models for passive scalars in isotropic turbulence, Physics of Fluids 15 (4) (2003) 961–985.
[27] S.B. Pope, Mapping closures for turbulent mixing and reaction, Theoretical and Computational Fluid Mechanics 2 (1991) 255–270.
[28] V. Eswaran, S.B. Pope, Direct numerical simulations of the turbulent mixing of a passive scalar, Physics of Fluids 31 (3) (1988) 506–520.
[29] A.T. Norris, S.B. Pope, Turbulent mixing model based on ordered pairing, Combustion and Flame 83 (1-2) (1991) 27–42.
[30] A.Y. Klimenko, S.B. Pope, The modeling of turbulent reactive flows based on multiple mapping conditioning, Physics of Fluids 15 (7) (2003) 1907–1925.
[31] M.J. Cleary, A. Kronenburg, Multiple mapping conditioning for extinction and reignition in turbulent diffusion flames, Proceedings of the Combustion Institute 31 (1) (2007) 1497–1505.
[32] A.P. Wandel, A.Y. Klimenko, Testing multiple mapping conditioning mixing for monte carlo probability density function simulations, Physics of Fluids 17 (12) (2005).
[33] D.W. Meyer, P. Jenny, A mixing model for turbulent flows based on parameterized scalar profiles, Physics of Fluids 18 (3) (2006).
[34] N. Peters, On the role of quasi-one-dimensional dissipation layers in turbulent scalar mixing, Tech. Rep., Center for Turbulence Research, 2002.
[35] L.P. Wang, N. Peters, The length-scale distribution function of the distance between extremal points in passive scalar turbulence, Journal of Fluid Mechanics 554 (2006) 457–475.
[36] R.R. Cao, H. Wang, S.B. Pope, The effect of mixing models in PDF calculations of piloted jet flames, Proceedings of the Combustion Institute 31 (1) (2007) 1543–1550.
[37] E.R. Hawkes, R. Sankaran, J.C. Sutherland, J.H. Chen, Scalar mixing in direct numerical simulations of temporally evolving plane jet flames with skeletal co/h2 kinetics, Proceedings of the Combustion Institute 31 (1) (2007) 1633–1640.

[38] R.O. Fox, On velocity-conditioned scalar mixing in homogeneous turbulence, Physics of Fluids 8 (10) (1996) 2678–2691.
[39] K. Liu, S.B. Pope, D.A. Caughey, Calculations of bluff-body stabilized flames using a joint probability density function model with detailed chemistry, Combustion and Flame 141 (1–2) (2005) 89–117.
[40] S.B. Pope, A Monte-Carlo method for the PDF equations of turbulent reactive flow, Combustion Science and Technology 25 (5-6) (1981) 159–174.
[41] D.W. Meyer, P. Jenny, Stochastic mixing model for PDF simulations of turbulent reactive flow, in: H.I. Andersson, P.A. Krogstad (Eds.), Tenth European Turbulence Conference, CIMNE, Trondheim, 2004, pp. 681–684.
[42] D.W. Meyer, P. Jenny, An improved mixing model providing joint statistics of scalar and scalar dissipation, Combustion and Flame 155 (3) (2008) 490–508.
[43] C.W. Gardiner, in: Handbook of Stochastic Methods for Physics, Chemistry and the Natural Sciences, third ed., Springer, Berlin, 2004.
[44] D.W. Meyer, P. Jenny, Consistent inflow and outflow boundary conditions for transported probability density function methods, Journal of Computational Physics 226 (2) (2007) 1859–1873.
[45] R.M. Heiberger, B. Holland, Statistical Analysis and Data Display an Intermediate Course with Examples in S-plus, R, and SAS, Springer, New York, 2004.